Pergamon

Journal of Structural Geology, Vol. 16, No. 2, pp. 253 to 262, 1994
Elsevier Science Ltd
Printed in Great Britain
0191-8141/94 $06.00+0.00

Strength of two-phase rocks: a model based on fiber-loading theory

SHAOCHENG JI and PINGLAO ZHAO

Département de géologie, Université de Montréal, C.P. 6128, Succursale "A", Montréal, Québec, Canada H3C 3J7

(*Received* 15 *September* 1992; *accepted in revised form* 22 *March* 1993)

Abstract—In order to predict the strength of two-phase rocks in terms of the component volume fraction, the aspect ratio of the strong phase and the strength contrast between the strong and weak phases, a simple model is developed according to a fiber-loading theory modified for short-fiber composites. The analytical solution derived from elastic theory is found to hold, in good approximation, for rocks consisting of power-law viscous minerals. There is a good agreement between the predicted results and the experiments for two-phase aggregates: anhydrite–halite, calcite–halite, Fe–Ag and clinopyroxene–plagioclase. The model is compared with several previous different models.

INTRODUCTION

BULK strength of composite rocks, in which a hard, relatively undeformable phase constitutes rigid inclusions dispersed in a ductile soft phase matrix, is usually considered as identical in value with that of the pure weak matrix component. It is a common practice, using the above approach, to predict the flow strength of the crust and upper mantle by extrapolating the steady-state laboratory flow law of quartz–plagioclase and olivine to natural strain-rates and temperatures (e.g. Kirby 1980, Carter & Tsenn 1987). However, because this approach does not take into consideration the strengthening behavior of the composites related to the interaction between hard phase and soft matrix, it underestimates the bulk flow stress even for rocks in which the weak phase is abundant with respect to the strong phase, and their strength contrast (strong/weak) is larger than 10/1.

In the scientific literature, numerous theoretical models have been developed to correlate strengthening mechanisms with microstructural characteristics of composites. These models are as follows.

(1) *Orowan strengthening effect*

If the second-phase particles are small enough to interact with single dislocations (i.e. grain size < several μm), the stiff particles can increase the strength of the composite material (Kelley 1973). The stiff particles act as impenetrable barriers to dislocation motion and force gliding dislocations to bow-out and by-pass them following the so-called Orowan mechanism (Orowan 1948). However, for relatively large particle size and spacing, which is the geological case discussed here, Orowan-type hardening would be negligible (Kelley 1973, Wu & Lavernia 1992).

(2) *Strengthening due to high dislocation density generated in the matrix around the strong inclusions*

Differences in thermal expansivities between different phases can lead to the generation of dislocations (increase in dislocation density) and to the reduction of subgrain size during changes in temperature (Arsenault & Shi 1986, Arsenault 1991, Dunand & Mortensen 1991). These microstructural changes may influence the material strength (Hirth & Tullis 1991, Ingrin *et al.* 1991).

(3) *Strengthening due to chemical reaction*

Chemical reaction between phases may lead to strengthening or weakening of rocks during prograde or retrograde metamorphism (Brodie & Rutter 1985).

(4) *Strengthening due to fiber-loading effect of strong phase grains in a soft matrix*

The theory of fiber-loading was developed by Cox (1952) and has been used to interpret extension fracture boudinage (Lloyd *et al.* 1982, Masuda & Kuriyama 1988, Ji & Zhao 1993). The theory can be briefly outlined as: the harder phase carries a comparatively greater part of the stress, while the soft phase tends to take the greater part of the strain (with reference to the volume fraction ratio).

While certainly not trivial, the effects of items (1)–(3) can, in principle, be treated with existing theory, and will not be considered further in this paper. Here, attention is focused on item (4), which has to date received little consideration by geologists but which will be shown to have a strong effect on the strength of rocks.

FIBER-LOADING THEORY FOR SHORT-FIBER COMPOSITES

Most crust and mantle rocks consist of two or more phases with different mechanical properties. Relevant examples are granite, diabase or gabbro, amphibolite, gneisses ranging from felsic to mafic in composition, peridotite and impure limestone or quartzite. Rocks may be classified into two types depending on the shape of rigid minerals: (i) short-fiber composites in which inequant rigid mineral grains such as feldspar, amphibole, pyroxene or tourmaline are dispersed in a ductilely deforming matrix consisting of soft minerals; and (ii) particle composites in which sphere-shaped rigid minerals are dispersed in a ductilely deforming, softer matrix. Relevant examples are garnet-bearing diatexitic mylonite and garnet–lherzolite.

To a first approximation, the microstructure of a two-phase rock may be represented by a hard cylindrical fiber with length l and diameter $2r$ with long axis parallel to the x-axis, completely embedded in a continuous soft matrix (Fig. 1). The aspect ratio of the fiber, $s = (l/2r)$, is greater than 1 for short-fiber composites and equal to 1 for particle composites. We use the fiber-loading model developed by Cox (1952). He assumed that the matrix as a whole is strained homogeneously, but that the state of uniform stress and strain is locally perturbed by transfer of load to the fiber. If P is the load in the fiber at a distance x from the end, Cox (1952) assumed

$$\frac{dP}{dx} = H(u - v), \tag{1}$$

where u is the longitudinal displacement in the fiber and v is the corresponding displacement the matrix would undergo if the fiber was absent; H is a constant.

In the regime of elastic deformation, according to Hooke's law, the load in the fiber is:

$$P = E_f A_f \frac{du}{dx}, \tag{2}$$

where E_f is Young's modulus, and A_f is the area of cross-section of the fibre, that is, $A_f = \pi r^2$.

Differentiating equation (1) and substituting equation (2) gives

$$\frac{d^2P}{dx^2} = H\left(\frac{P}{E_f A_f} - \varepsilon\right), \tag{3}$$

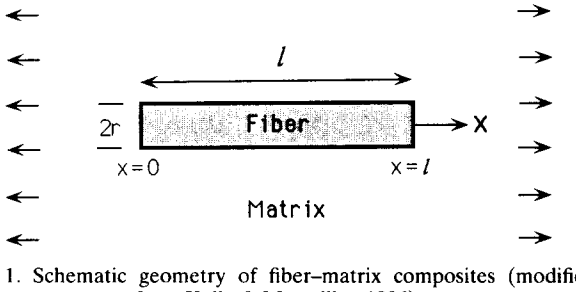

Fig. 1. Schematic geometry of fiber–matrix composites (modified from Kelly & Macmillan 1986).

where $\varepsilon = (dv/dx) =$ constant. This differential equation is solved as

$$P(x) = E_f A_f \varepsilon + S_1 \sinh \beta x + S_2 \cosh \beta x, \tag{4}$$

where S_1 and S_2 are constants, and according to Cox (1952) and Kelly & Macmillan (1986, pp. 261),

$$\beta = \left(\frac{2\pi G_m}{E_f A_f \ln R/r}\right)^{1/2}, \tag{5}$$

where G_m is the shear modulus of the matrix, and R is half the average spacing between fibers.

For long fibers, the model of Cox (1952) assumes no load transfer from the matrix to the end faces of the fiber, that is, $P(0) = P(l) = 0$. However, for short fibers, the load transfer at the ends cannot be ignored because the aspect ratio significantly affects stress magnitude and distribution in the fiber (Tyson & Davies 1965, Nardone & Prewo 1986). Therefore, we set the boundary conditions as:

$$P(0) = P(l) = \pi r^2 \sigma_i, \tag{6}$$

where σ_i is the stress acting on the fiber ends, $\sigma_i = E_m \varepsilon$ (Nardone & Prewo 1986, Wu & Lavernia 1992, Zhao & Ji 1992), and E_m is the Young's modulus of the matrix.

Substituting equation (4) into equation (6), the distribution of tensile stress in the fiber is then:

$$\sigma_f(x) = \left\{\frac{E_f}{E_m} + \left(1 - \frac{E_f}{E_m}\right)\frac{\cosh[\beta(l/2 - x)]}{\cosh(\beta l/2)}\right\}\sigma_i \tag{7}$$

and the average stress in the fiber is

$$\bar{\sigma}_f = \frac{\int_0^l \sigma_f(x)\,dx}{l} = \left[\frac{E_f}{E_m} + \left(1 - \frac{E_f}{E_m}\right)\frac{\tanh \psi}{\psi}\right]\sigma_i, \tag{8}$$

where

$$\psi = \frac{\beta l}{2} = s\left[\frac{-2E_m}{E_f(1 + \nu)\ln(F_f)}\right]^{1/2} \tag{9}$$

and where F_f and ν are the volume fraction of the fibers in the composite and Poisson's ratio of the matrix, respectively.

The average stress on the composite is

$$\begin{aligned}\sigma_c &= F_f \bar{\sigma}_f + F_m \bar{\sigma}_m \\ &= F_f\left\{\frac{E_f}{E_m} + \left(1 - \frac{E_f}{E_m}\right)\frac{\tanh \psi}{\psi}\right\}\sigma_i \\ &\quad + (1 - F_f)\bar{\sigma}_m,\end{aligned} \tag{10}$$

where $F_f + F_m = 1$. The average stress acting on the matrix, $\bar{\sigma}_m$, will be σ_i assuming no slip at the fiber–matrix interface (Nardone & Prewo 1986). Therefore,

$$\frac{\bar{\sigma}_c}{\bar{\sigma}_m} = F_f\left\{\frac{E_f}{E_m} + \left(1 - \frac{E_f}{E_m}\right)\frac{\tanh \psi}{\psi}\right\} - F_f + 1. \tag{11}$$

According to Nardone & Prewo (1986) and Taya & Arsenault (1987), the yield strength of the composite occurs when the matrix reaches its yield strength (S_m), that is, $\bar{\sigma}_m = S_m$. This implies that the addition of fibers increases the strength of composite, but does not in-

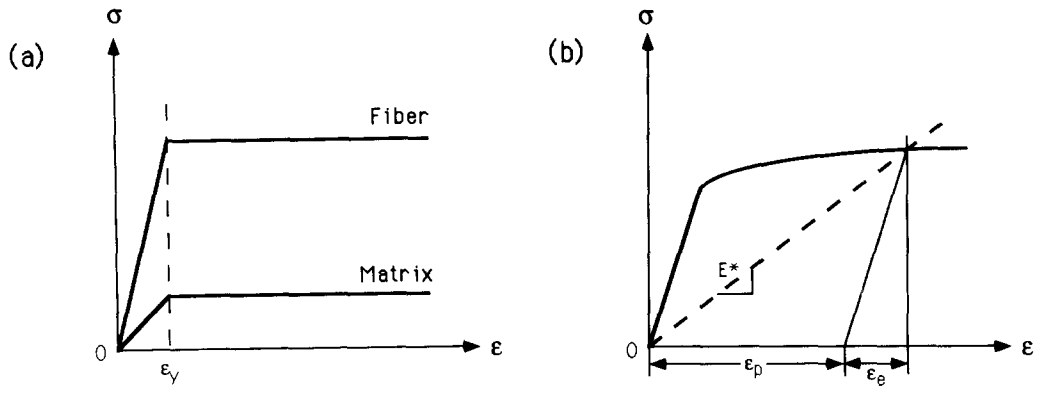

Fig. 2. Stress–strain curves at imposed strain-rate and constant temperature. (a) Perfectly elastoplastic materials. (b) Power-law viscous materials. The indicated σ–ε points on the elastic–plastic stress–strain diagram (solid lines) may also be reached with an elastic model material (dashed lines). The corresponding elastic constants (E^* and ν^*) can be evaluated for each σ–ε point, the total strain ε being the sum of the elastic strain ε_e and the plastic strain ε_p.

crease the strength of matrix since the strengthening of the composite matrix by dislocation generation is ignored. Therefore, we obtain

$$\frac{S_c}{S_m} = \frac{\bar{\sigma}_c}{\bar{\sigma}_m} = F_f\left\{\frac{E_f}{E_m} + \left(1 - \frac{E_f}{E_m}\right)\frac{\tanh \psi}{\psi}\right\} - F_f + 1, \quad (12)$$

where S_c is the yield strength of composite.

Equation (12) was derived from elastic theory. In the following paragraphs, we will determine the applicability of the analytical elastic solutions when a composite rock undergoes plastic flow.

(1) The elastic solution of equation (12) can be used to describe the flow strength of composite if the following two conditions are satisfied: (i) both the fiber and the matrix in the composite are perfectly elastoplastic materials (Obert & Duvall 1967), i.e. they are linear-elastic below the yield strain and are perfectly plastic without strain hardening or weakening above the yield strain (Fig. 2a); and (ii) the fiber and the matrix have similar yield strains at given temperature, pressure and strain-rate. An investigation of the scientific literature shows that the second approximation is formally correct (e.g. Paterson 1978, Jaeger & Cook 1979, Kirby & McCormick 1984, Poirier 1985). Under these conditions, E_f/E_m is approximated to be equal to the ratio (ξ) of fiber flow strength to matrix flow strength. Then equation (12) can be written as

$$\frac{S_c}{S_m} = F_f\left\{\xi + (1 - \xi)\frac{\tanh\left[s\left(\frac{-2}{\xi(1+\nu)\ln(F_f)}\right)^{1/2}\right]}{s\left(\frac{-2}{\xi(1+\nu)\ln(F_f)}\right)^{1/2}}\right\} - F_f + 1, \quad (13)$$

where S_c and S_m become the flow strength or yield strength for the composite and the matrix, respectively.

(2) Even if the fiber and the matrix are power-law materials, equation (12) may still stand when actual composite material which is elastically and plastically deformed to a certain point can be replaced by an elastic model material reaching the same point of stress and strain (Poech's approximation, Poech 1992) (Fig. 2b). In this case, however, E in equation (12) and ν in equation (9) should be replaced by a secant Young's modulus (E^*) and a corresponding Poisson ratio (ν^*), respectively. E^* and ν^* are given:

$$E^* = \frac{\sigma}{\varepsilon} = \frac{\sigma}{\varepsilon_e + \varepsilon_p} \quad (14)$$

$$\nu^* = \frac{\nu\varepsilon_e + 0.5\varepsilon_p}{\varepsilon_e + \varepsilon_p}, \quad (15)$$

where σ is the stress, ε_e and ε_p are the elastic and plastic strains, respectively (Fig. 2b). With the above approximation, E_f^*/E_m^* is also found to be equal to ξ, where E_f^* and E_m^* are the secant Young's modulus for the fiber and the matrix, respectively. Thus we assume that equation (13) can be used to describe the flow strength of composite rocks consisting of power-law viscous phases.

From equation (13), we can predict: (i) a strengthening effect for a two-phase composite with increasing aspect ratio of the hard phase (Fig. 3a); (ii) a substantial increase in strength of the composite with increasing volume fraction of the hard phase (Figs. 3a & b); and (iii) effects of strength contrast (ξ) between the fiber and the matrix on strengthening of the composite (Fig. 3b). As shown in Fig. 3(b), for small aspect ratio (i.e. $s = 1$) there is a dramatic increase in the bulk strength of the particle composites when $F_f \geq 0.80$, but this sharp rise at large F_f diminishes as the fiber aspect ratio, s, increases. When $s \geq 10$, the relationship between S_c/S_m and F_f becomes linear (Fig. 3a).

COMPARISON WITH EXPERIMENTS

At laboratory strain-rates (10^{-4}–10^{-6} s^{-1}), most geological materials undergo rather semi-brittle creep than perfect plastic deformation without change of volume. Thus, ν^* should be smaller than 0.5. We found that $\nu^* = 0.25$ led to the best agreement between the predicted results and experimental ones.

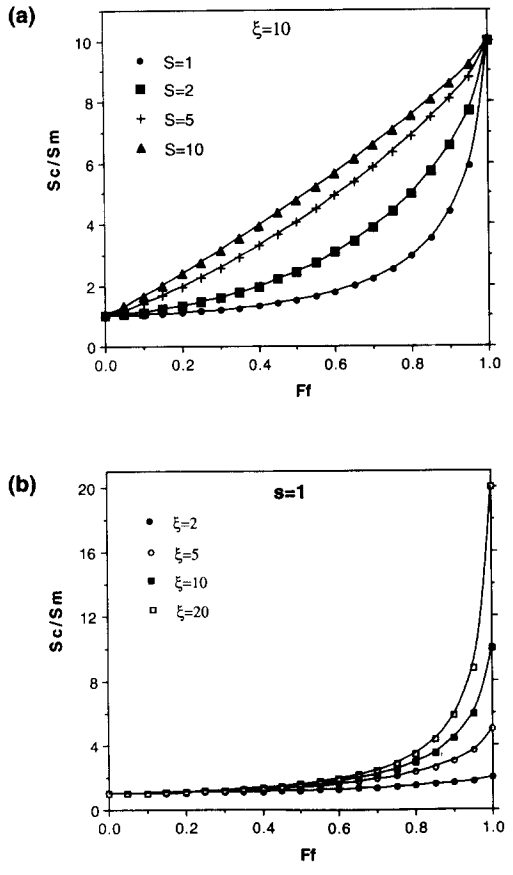

Fig. 3. S_c/S_m (ratio of the composite strength to the matrix strength) as a function of F_f (fiber volume fraction), predicted by the fiber-loading model. (a) Effects of fiber aspect ratio (s) on S_c/S_m for a given ξ (strength contrast between the two pure phases) of 10. (b) Influences of ξ on S_c/S_m for a given s.

Anhydrite–halite aggregates (Price 1982)

In order to test the model developed in the previous section, we have selected Price's (1982) experimental results for comparison. His samples were sintered anhydrite–halite aggregates with a varied anhydrite volume fraction (0, 0.25, 0.50, 0.75, 1.00). The deformation experiments were performed at a temperature of 200°C and a strain-rate of 10^{-4} s^{-1}. At the experimental conditions, halite was deformed by intracrystalline plasticity and anhydrite by a combination of intracrystalline plasticity and microfracturation. Figures 4(a) & (b) show the sample strength at 10% axial strain as a function of anhydrite volume fraction (F_f) at confining pressures of 100 and 200 MPa, respectively. A dramatic increase in bulk strength occurs when $F_f \geq 0.80$. Although information about the anhydrite aspect ratio (s) in the samples is not available from Price (1982), the ratio of the composite strength to the pure soft matrix strength (S_c/S_m) predicted by our model based on $s = 1$ is in good agreement with Price's experimental results (Fig. 4).

Calcite–halite aggregates (Jordan 1987, 1988)

Sets of calcite–halite aggregates with calcite contents varying from 0 to 100% were artificially made by sintering, and then were deformed coaxially at confining pressures of 150, 200 and 250 MPa, temperatures of 20 and 200°C, and a strain-rate of 10^{-4} s^{-1} (Jordan 1988). At all experimental conditions, halite was soft and deformed by crystal plasticity while calcite was hard and semi-brittle. The strength contrast between calcite and halite increased with increasing confining pressure (Fig. 5b). The strength vs F_f, and S_c/S_m vs F_f plots are shown in the left and right columns of Fig. 5, respectively. Jordan's experimental results fit well the predicted $S_c/S_m - F_f$ relationship based on $s = 2$. Examination of the microstructural photographs in Jordan (1987) shows that the calcite grains in his samples had an average aspect ratio of about 2.

Iron–silver aggregates (Le Hazif 1978)

Le Hazif (1978) deformed pure Fe and pure Ag aggregates and sintered Fe–Ag aggregates containing phases of equal volume fractions at room temperature and pressure, and a strain-rate of 7×10^{-5} s^{-1}. Microstructural observation shows that the Fe and Ag phases in the undeformed sintered aggregates are closely interconnected and that the Fe phase is almost equigranular (i.e. $s = 1$). At a given strain of 10%, the strengths of the pure Fe and pure Ag aggregates, and the two-phase aggregate are 43, 19 and 23 kg mm^{-2}, respectively (Fig. 6a). Le Hazif's experimental results agree well with our model prediction for $s = 1$ (Fig. 6b).

Diabase (Shelton & Tullis 1981)

Shelton & Tullis (1981) experimentally determined the power flow laws in axial compression for plagioclase, clinopyroxene and diabase (64% cpx, 36% pl). In the experimental conditions, clinopyroxene is stronger than plagioclase. Individual clinopyroxene grains in the diabase are fairly equant (J. Tullis personal communication). These flow laws are:

$$\dot{\varepsilon} = 1.18 \times 10^6 \text{ s}^{-1}\text{GPa}^{-3.9}\sigma^{3.9} + \exp\left(\frac{-234 \text{ kJ mol}^{-1}}{RT}\right) \quad (16)$$

for plagioclase,

$$\dot{\varepsilon} = 9.95 \times 10^8 \text{ s}^{-1}\text{GPa}^{-2.6}\sigma^{2.6} + \exp\left(\frac{-335 \text{ kJ mol}^{-1}}{RT}\right) \quad (17)$$

for clinopyroxene and

$$\dot{\varepsilon} = 2.58 \times 10^6 \text{ s}^{-1}\text{GPa}^{-3.4}\sigma^{3.4} + \exp\left(\frac{-260 \text{ kJ mol}^{-1}}{RT}\right) \quad (18)$$

for diabase.

As shown in Fig. 7, the relative strength of diabase ($F_f = 0.64$) with respect to plagioclase strength, calculated from flow law equations (16)–(18) at 800 and 900°C and

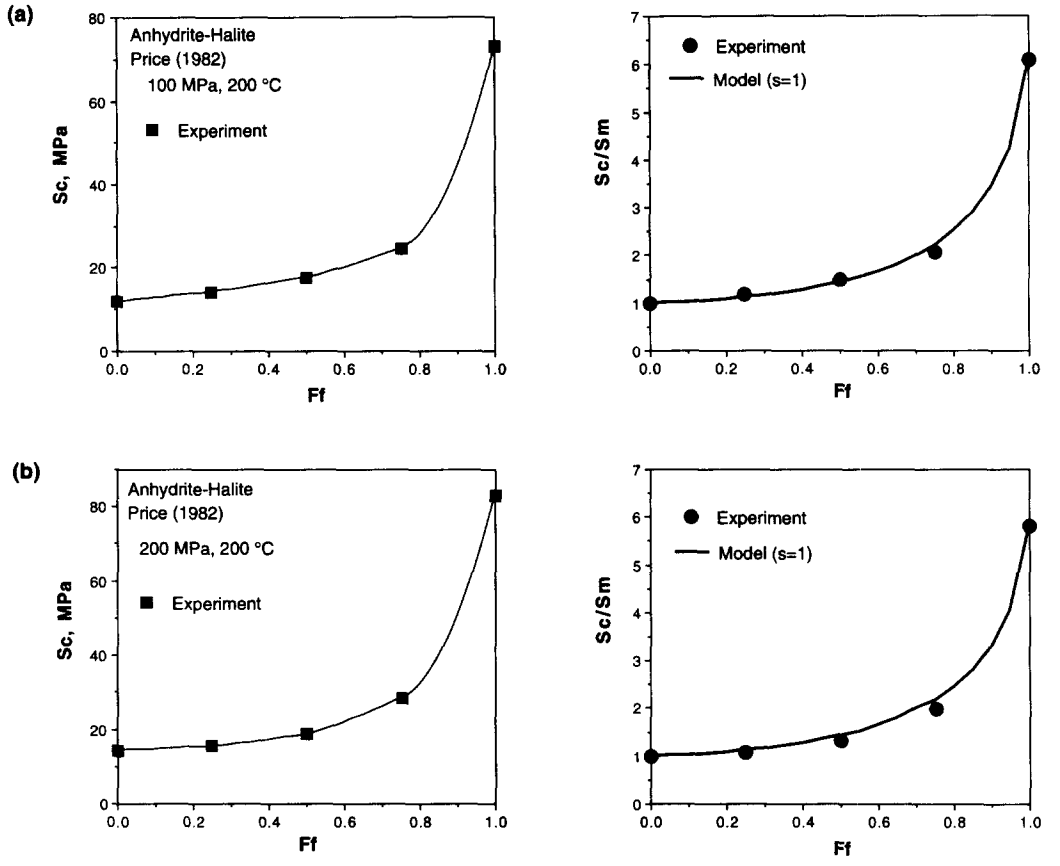

Fig. 4. Results of experimental investigations on anhydrite–halite aggregates (composite strength, S_c, vs the strong phase volume fraction, F_f, in the left column) compared with the model predictions based on $s = 1$ (in the right column). Data from Price (1982). (a) Strengths for a given strain of 10% at a temperature of 200°C, a confining pressure of 100 MPa and a strain-rate of $10^{-4}\,s^{-1}$. (b) Strengths for a given strain of 10% at a temperature of 200°C, a confining pressure of 200 MPa and a strain-rate of $10^{-4}\,s^{-1}$

a strain-rate of $10^{-6}\,s^{-1}$, agrees very well with our model prediction for $s = 1$.

In summary, the bulk strength of two-phase composites predicted by the fiber-loading theory was found to be quite consistent with the experimentally observed strength for anhydrite–halite (Price 1982), calcite–halite (Jordan 1987, 1988), Fe–Ag (Le Hazif 1978) and clinopyroxene–plagioclase (Shelton & Tullis 1981) aggregates. The materials science literature does contain additional experimental studies on the bulk flow strengths of composites as functions of both volume fraction and aspect ratio of the strong phase (e.g. Arsenault 1991, Kim & Chou 1987, Taya & Arsenault 1989, Pachalis & Chou 1992, Wu & Lavernia 1992). However, it is not appropriate to compare the present model to these studies because the diameter of hard fibers or particulates is so small (< several μm) that dislocation-related strengthening is important. In such cases both the fiber-loading effect and dislocation-related strengthening should be taken into consideration (Wu & Lavernia 1992). Therefore, further testing of the proposed model will require systematic studies on the experimental deformation of synthetic bi-phase rocks with controlled volume fraction, aspect ratio of the rigid component and strength contrast between two component phases.

COMPARISON WITH OTHER MODELS

Comparison with Tharp (1983) *model*

Tharp (1983) suggested that a two-phase rock, in which the stronger mineral constitutes a load-carrying framework and $\xi \geq 10$, could be modelled by analogy with porous powder metals. This so-called Tharp model predicts the following bulk strength of the aggregate (S_c):

$$\frac{S_c}{S_m} = \xi[1 - k(1 - F_f)^{2/3}], \qquad (19)$$

where ξ is the strength contrast between the two pure phases and k is a geometrical coefficient which depends on a number of factors such as the shape and configuration of the weak phase, ξ and the deformation mechanism, and therefore the temperature, etc. (Jordan 1988, Handy 1990). k ranges from 0.98 to 3.8 (Griffiths *et al.* 1979). Tharp (1983) found that $k = 1.8$ represents a good fit to empirical tensile strengths of various sintered porous metals, whereas Jordan (1987) found that $k = 1.1$–1.5 for the strengths of calcite–halite and anhydrite–halite compressed coaxially in a pseudo-triaxial ($\sigma_1 > \sigma_2 = \sigma_3$) configuration.

As shown in Fig. 8, comparisons between the Tharp

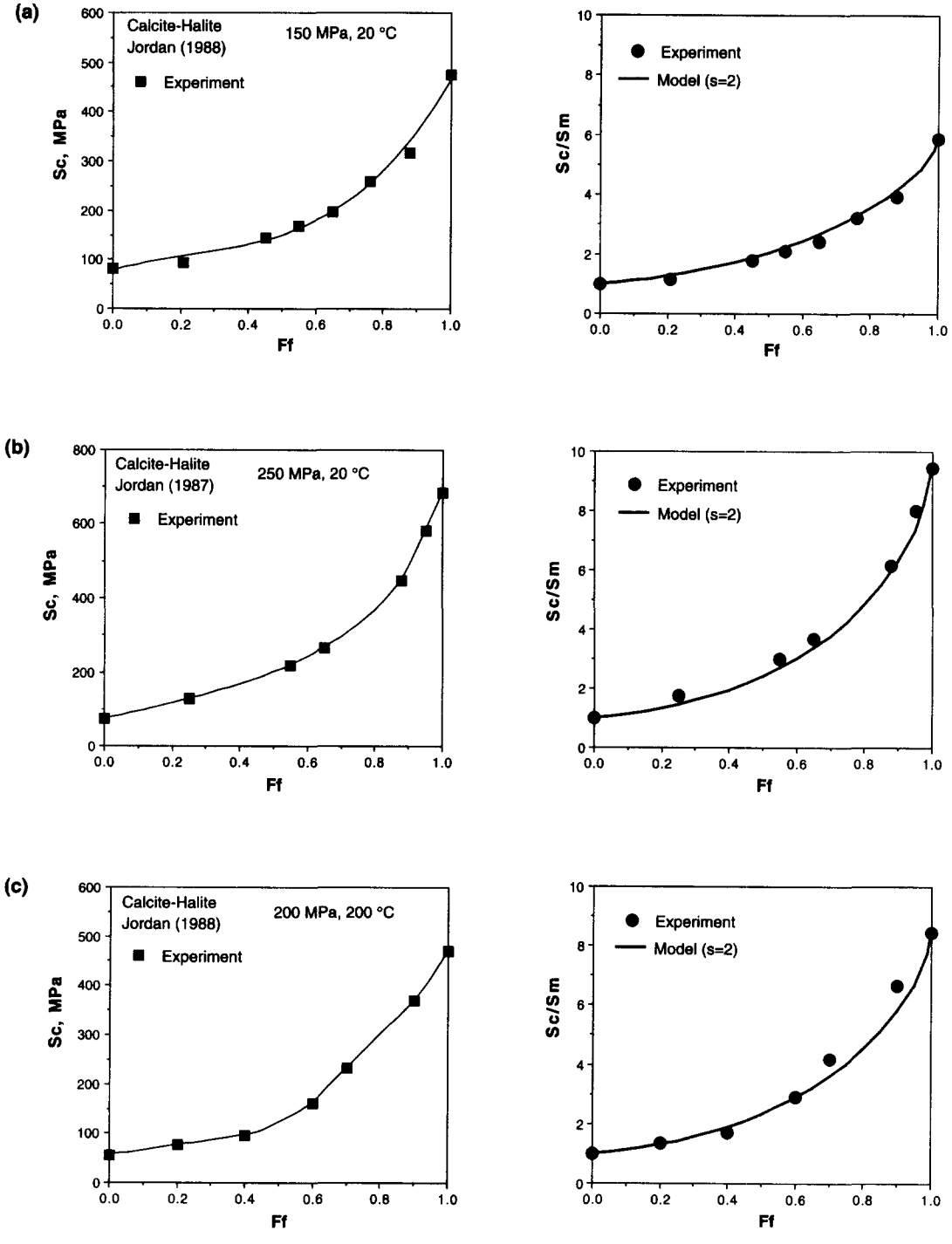

Fig. 5. Results of experimental investigations on calcite–halite aggregates (S_c vs F_f, in the left column) compared with the model predictions based on $s = 2$ (in the right column). Data from Jordan (1987, 1988). (a) Strengths for a given strain of 20% at a temperature of 20°C, a confining pressure of 150 MPa and a strain-rate of 10^{-4} s^{-1}. (b) Strengths for a given strain of 6% at 20°C, a confining pressure of 250 MPa and a strain-rate of 10^{-4} s^{-1}. (c) Strengths for a given strain of 20% at 200°C, confining pressure 200 MPa and strain-rate 10^{-5} s^{-1}.

model and the present model reveal two points: (i) in composites consisting of a ductile matrix with an intermediate to low volume fraction of strong phase, the strong phase cannot form a load-carrying framework; most of the matrix may deform freely while perturbation takes place only in a small area around the inclusions. This case cannot be modelled by the Tharp model, which is limited to rocks with $F_f \geq 0.75$; and (ii) although the strengthening effect predicted by the Tharp model is very close to that predicted by the present model for composites with F_f between 0.75 and 1.00, the value of s offers more direct information about the shape of the strong phase than the value of k.

Comparison with Duva (1984) model

Duva (1984) considered theoretically the strengthening effect of rigid (undeformable) spherical inclusions on a power-law viscous matrix (strength contrast $\xi \geq 10$). The inclusions have to be large enough that their inter-

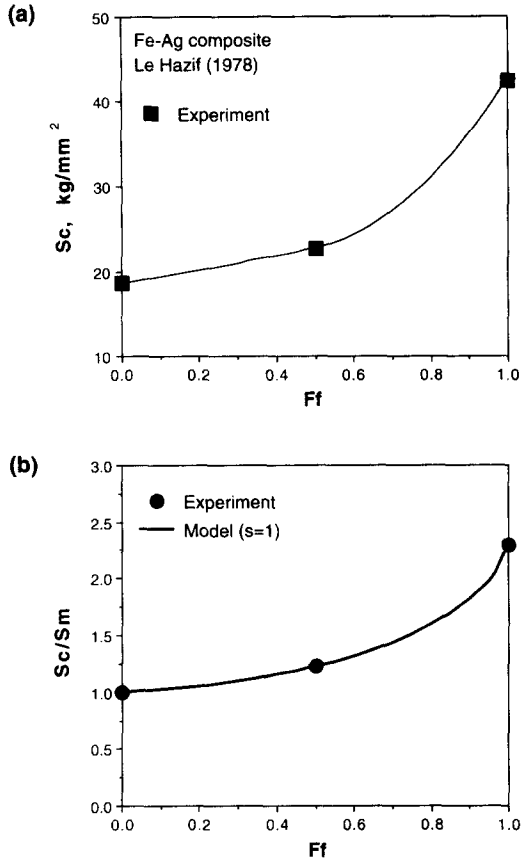

Fig. 6. Results of experimental investigations on (a) Fe–Ag aggregates (S_c vs F_f) compared with the model predictions based on $s = 1$ (b). Data from Le Hazif (1978). Strengths for a given strain of 10% at 25°C, confining pressure 0.1 MPa and strain-rate 7×10^{-5} s^{-1}.

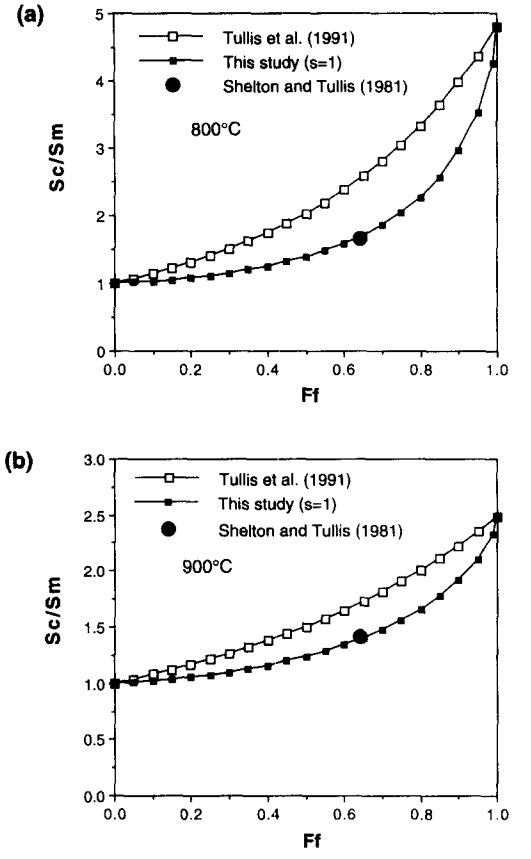

Fig. 7. Flow strengths of the clinopyroxene–plagioclase aggregate as a function of pyroxene volume fraction at (a) 800°C and (b) 900°C, and a strain-rate of 10^{-6} s^{-1}, predicted by the model of Tullis *et al.* (1991), compared with those predicted by the fiber-loading model (this study). Flow strength of diabase (64% cpx, 36% pl) calculated from Shelton & Tullis (1981) is indicated by a dot.

action with the matrix can be characterized by continuum plasticity (Chen & Argon 1979, Fleck *et al.* 1989). That is, they must be at least several microns in size rather than those, like fine precipitates, small enough to interact with single dislocations. Duva's model leads to a prediction for the overall flow stress (S_c) of a composite material in pure-shear with a dilute distribution (i.e. $F_f < 0.3$) of rigid spherical particles (see Duva (1984) for details):

$$S_c = \frac{S_m}{(1 - F_f)^{0.48}}, \tag{20}$$

where S_m is the flow stress for the matrix without rigid inclusions, and F_f is the volume fraction of the rigid particles.

We compared the strengthening effect predicted by the Duva model with that predicted by our model. $\xi = 10$ and $s = 1$ were used in our modelling; this is consistent with Duva's model (i.e. the inclusions are rigid spherical particles). As shown in Fig. 9, the values predicted here are only about 3% lower than the values derived by the Duva model.

Comparison with model of Tullis et al. (1991)

A finite-element modelling study allowed Tullis *et al.* (1991) to propose that the flow law for a two-phase composite can be approximated by a power flow law in the same form as those for the end-member components:

$$\dot{\varepsilon} = A\sigma^n \exp\left(\frac{-Q}{RT}\right), \tag{21}$$

where $\dot{\varepsilon}$ is the strain-rate, σ is the differential flow stress, n, Q and A represent the power-law exponent, activation enthalpy and pre-exponential factor, respectively, R is the gas constant, and T is absolute temperature.

Tullis *et al.* (1991) assumed that the log of the compo-

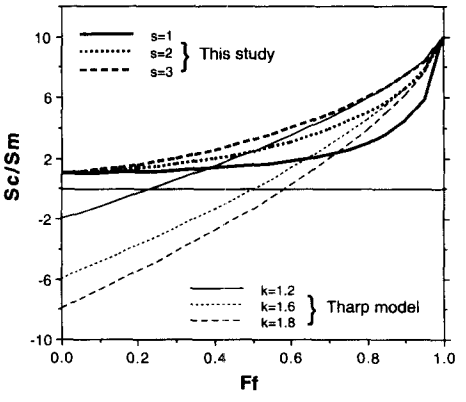

Fig. 8. A comparison of the fiber-loading model (this study) and the Tharp model.

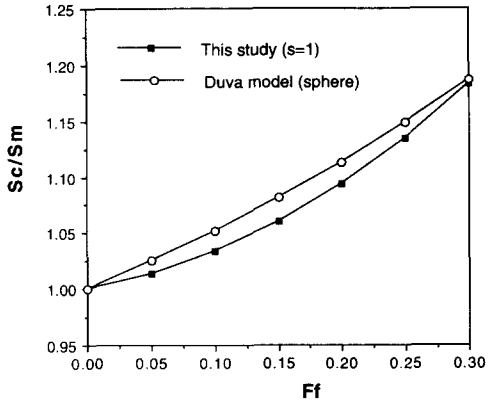

Fig. 9. A comparison of the fiber-loading model (this study) and the Duva model.

site stress exponent falls between the logs of the end-member stress exponents in proportion to the volume fraction of the end-members in the composite, that is, $\log n_c = F_f \log n_f + F_m \log n_m$, and obtained the composite flow law parameters n_c, Q_c and A_c from the following three equations:

$$n_c = 10^{(F_f \log n_f + F_m \log n_m)} \quad (22)$$

$$Q_c = \frac{Q_m(n_c - n_f) - Q_f(n_c - n_m)}{n_m - n_f} \quad (23)$$

$$A_c = 10^{[(n_c - n_f)\log A_m (n_c - n_m)\log A_f]/(n_m - n_f)}, \quad (24)$$

where the subscripts c, f and m stand for the composite, the strong phase and the weak phase, respectively, and F represents volume fraction. Comparison between the values of S_c/S_m predicted by the model of Tullis *et al.* (1991) and those by the present model for clinopyroxene–plagioclase aggregate as a function of pyroxene volume fraction at 800 and 900°C and 10^{-6} s^{-1} are given in Figs. 7(a) & (b). Some difference exists between the results of these two models, but that by the present model seems to match better with the experimental result of Shelton & Tullis (1981) on diabase (64% cpx, 36% pl).

In summary. (i) There have been a number of attempts to estimate two-phase composite strengths (Tharp 1983, Jordan 1988, Handy 1990, Tullis *et al.* 1991). Unlike the above studies, the present study has attempted to obtain an approximate analytical solution for composite strength as a function of the constituent volume fraction, the strength contrast between the two pure phases, and the aspect ratio of the hard phase. (ii) The proposed model can be applied to predict the strength of two-phase composites with F_f ranging from 0 to 1, whereas the Tharp model is restricted to composites with $F_f > 0.75$, and Duva model to $F_f < 0.3$.

DISCUSSION

There are four cautions in using the model developed in this paper to predict composite strength.

(1) The model is based on the assumption that uniformly distributed short fibers are embedded in a ductile matrix. However, in tectonites, particularly rocks that have experienced low strain, the elongate rigid grains are not perfectly aligned parallel to the extensional direction. Therefore, the predicted values should be viewed as an upper limit to the bulk composite strength. The divergence of the predicted value from the measured value should diminish with decreasing aspect ratio of the hard phase.

(2) In the model, it is assumed that the fiber–matrix interfacial strength was high enough to resist debonding and slipping. Under low confining pressure, however, voids or cracks may nucleate along grain boundaries between the strong and weak phases, resulting in a reduction of the bulk flow strength of the composite (Nutt & Needleman 1987, Fleck *et al.* 1989). Therefore, the predicted flow strength should be compared with those values measured at high confining pressure. If all the interfaces between the fiber and matrix can slip freely, the matrix of the composite deforms as does unreinforced matrix, and therefore $S_c = S_m$ (McLean 1972).

(3) The strength contrast between two phases also affects composite strength. In contrast to high strength matrix, low strength matrix has stronger ductility and is able to accommodate a large stress concentration, without the nucleation of cracks, in the vicinity of matrix–fiber interfaces (Shang *et al.* 1988, Wu & Lavernia 1992).

(4) The application of analytical elastic solutions to plastic flow was based on Poech's approximation that actual composite material which is elastically and plastically deformed to a certain point can be replaced by an elastic model material reaching the same point of stress and strain (Poech 1992). In spite of the fact that the agreement between the model and the experiments is satisfactory for two-phase aggregates consisting of anhydrite–halite, calcite–halite, Fe–Ag and clinopyroxene–plagioclase (Figs. 4–7), further work is needed on common silicate rocks.

As a by-product, it should be pointed out that the differential flow stress estimated from microstructural piezometers (dynamically recrystallized grain size, subgrain size and dislocation density) (e.g. Twiss 1977, Derby 1991) in the soft phase matrix (e.g. Hacker *et al.* 1992) cannot be considered to be the bulk flow stress of two-phase composite rocks. This is because the distribution of stresses and strains in the two-phase composites is not homogeneous: the harder phase carries a comparatively greater stress, while the softer phase tends to take the greater part of the strain.

CONCLUDING REMARKS

(1) The simple model presented in this paper allows prediction of the flow strength of two-phase rocks as a function of the component volume fraction, the aspect ratio of the strong phase, and the strength contrast between the two phases. The agreement with experi-

ments is satisfactory for two-phase aggregates consisting of anhydrite–halite, calcite–halite, Fe–Ag and clinopyroxene–plagioclase. Thus if one knows the strength of quartz, feldspar, amphibole, pyroxene and olivine monomineralic aggregates and their average aspect ratio, one can calculate, to a first approximation, strengths for large portions of the lower crust and upper mantle.

(2) The model may be used to account for the flow strength of composites containing any volume fraction of strong phase. Although the Tharp model and the Duva model can predict the strength of composites, the Tharp model is restricted to rocks with a high volume fraction of the strong phase ($F_f > 75\%$) and the Duva model is limited to $F_f < 30\%$. The earlier models did not take into consideration the effect of strong phase aspect-ratio on the strength of composites.

(3) The model is thought to be valid for two-phase rocks with relatively coarse crystals of the strong phase ($>10\ \mu m$). For rocks with a fine-grained strong phase, the dislocation-related strengthening effect (Kelley 1973, Taya & Arsenault 1989) may be substantial, and thus both the fiber-loading effect and the dislocation-related strengthening effect should be taken into account in predicting the flow stress of composite rocks.

Acknowledgements—This study was supported by grants from the NSERC of Canada, FCAR of Québec and Université de Montréal to S. Ji. We thank Drs J. Tullis, W. Trzcienski and J. Martignole for helpful discussion of an early version of this manuscript, and Dr T. M. Tharp and an anonymous referee for constructively reviewing the manuscript.

REFERENCES

Arsenault, R. J. 1991. Strengthening of metal matrix composites due to dislocation generation through CTE mismatch. In: *Metal Matrix Composites: Mechanisms and Properties* (edited by Everett, R. K. & Arsenault, R. J.). ARC Press, 79–100.

Arsenault, R. J. & Shi, N. 1986. Dislocation generation due to differences between the coefficients of thermal expansion. *Mater. Sci. Engng* **81**, 175–187.

Brodie, K. H. & Rutter, E. H. 1985. On the relationship between deformation and metamorphism, with special reference to the behavior of basic rocks. In: *Metamorphic Reactions: Kinetics, Textures and Deformation* (edited by Thompson, A. B. & Rubie, D. C.). Springer, New York, 138–179.

Carter, N. L. & Tsenn, M. C. 1987. Flow properties of continental lithosphere. *Tectonophysics* **136**, 27–63.

Chen, I. W. & Argon, A. S. 1979. Steady state power law creep in heterogeneous alloys with coarse microstructures. *Acta metall.* **27**, 785–791.

Cox, H. L. 1952. The elasticity and strength of paper and other fibrous materials. *Br. J. appl. Phys.* **3**, 72–79.

Derby, B. 1991. The dependance of grain size on stress during dynamic recrystallization. *Acta metall. Mater.* **39**, 955–962.

Dunand, D. & Mortensen, A. 1991. Dislocation emission at fibers—I. Theory of longitudinal punching by thermal stresses. *Acta metall. Mater.* **39**, 1405–1416.

Duva, J. M. 1984. A self-consistent analysis of the stiffening effect of rigid inclusions on a power-law material. *J. Engng Mater. Technol.* **106**, 317–321.

Fleck, N. A., Hutchinson, J. W. & Tvergaard, V. 1989. Softening by void nucleation and growth in tension and shear. *J. Mech. Phys. Solids* **37**, 515–540.

Griffiths, T. J., Davies, R. & Bassett, M. B. 1979. Analytical study of effects of pore geometry on tensile strength of porous materials. *Powder metall.* **22**, 119–123.

Hacker, B. R., Yin, A., Christie, J. M. & Davis, G. A. 1992. Stress magnitude, strain rate, and rheology of extended middle continental crust inferred from quartz grain sizes in the Whipple Mountains, California. *Tectonics* **11**, 36–46.

Handy, M. R. 1990. The solid-state flow of polymineralic rocks. *J. geophys. Res.* **95**, 8647–8661.

Hirth, G. & Tullis, J. 1991. The effect of porosity on the strength of quartz aggregates experimentally deformed in the dislocation creep regime. *Tectonophysics* **200**, 97–110.

Ingrin, J., Doukhan, N. & Doukhan, J. C. 1991. High-temperature deformation of diopside single crystal, 2. Transmission electron microscopy investigation of the defect microstructures. *J. geophys. Res.* **96**, 14,287–14,297.

Jaeger, J. C. & Cook, N. G. W. 1979. *Fundamentals of Rock Mechanics* (3rd edn). Chapman and Hall, London.

Ji, S. & Zhao, P. 1993. Location of tensile fracture within rigid–brittle inclusions in ductilly flowing matrix. *Tectonophysics* **220**, 23–31.

Jordan, P. 1987. The deformational behaviour of bimineralic limestone–halite aggregates. *Tectonophysics* **135**, 185–197.

Jordan, P. 1988. The rheology of polymineralic rocks—an approach. *Geol. Rdsch.* **77**, 285–294.

Kelley, P. M. 1973. The quantitative relationship between microstructure and properties in two-phase alloys. *Int. metall. Rev.* **18**, 31–36.

Kelly, A. & Macmillan, N. H. 1986. *Strong Solids*. Oxford Science Publications, Oxford.

Kim, J. & Chou, T.-W. 1987. Creep analysis of ceramic matrix composites. In: *Proceedings of the American Society for Composites*. Technomic Publishing Co., 303–309.

Kirby, S. H. 1980. Tectonic stresses in the lithosphere: Constraints provided by experimental deformation of rocks. *J. geophys. Res.* **85**, 6353–6363.

Kirby, S. H. & McCormick, J. W. 1984. Inelastic properties of rocks and minerals: strength and rheology. In: *Handbook of Physical Properties of Rocks, Volume* 3 (edited by Carmichael R. S.). CRC Press, Boca Raton, Florida.

Le Hazif, R. 1978. Déformation plastique du systeme biphase fer–argent de composition equivolumique. *Acta metall.* **26**, 247–257.

Lloyd, G. E., Ferguson, C. C. & Reading, K. 1982. A stress-transfer model for the development of extension fracture boudinage. *J. Struct. Geol.* **4**, 355–372.

Masuda, T. & Kuriyama, M. 1988. Successive "mid-point" fracturing during microboudinage: an estimate of the stress–strain relation during a natural deformation. *Tectonophysics* **147**, 171–177.

Nardone, V. C. & Prewo, K. M. 1986. On the strength of discontinuous silicon carbide reinforced aluminum composites. *Scr. metall.* **20**, 43–48.

Nutt, S. R. & Needleman, A. 1987. Void nucleation at fiber ends in Al–SiC composites. *Scr. metall.* **21**, 705–710.

McLean, D. 1972. Viscous flow of aligned composites. *J. Mater. Sci.* **7**, 98–104.

Obert, J. & Duvall, W. I. 1967. *Rock Mechanics and the Design of Structures in Rock*. John Wiley & Sons, London.

Orowan, E. 1948. *Symposium on Internal Stresses in Metals and Alloys, London*.

Pachalis, J. R. & Chou, T.-W. 1992. Modeling of creep of misaligned short-fiber reinforced ceramic composites. *J. appl. Mech.* **59**, 27–32.

Paterson, M. S. 1978. *Experimental Rock Deformation—The Brittle Field*. Springer, New York.

Poech, M. H. 1992. Deformation of two-phase materials: application of analytical elastic solutions to plasticity. *Scr. metall. Mater.* **27**, 1027–1031.

Poirier, J. P. 1985. *Creep of Crystals*. Cambridge University Press, Cambridge.

Price, R. H. 1982. Effects of anhydrite and pressure on the mechanical behaviour of synthetic rocksalt. *Geophys. Res. Lett.* **9**, 1029–1032.

Shang, J. K., Yu, W. & Richie, R. O. 1988. Role of silicon carbide particles in fatigue crack growth in SiC-particular-reinforced aluminum alloy composites. *Mater. Sci. Engng* **102A**, 181–192.

Shelton, G. L. & Tullis, J. 1981. Experimental flow laws for crustal rocks. *Eos* **62**, 396.

Taya, M. & Arsenault, R. J. 1987. A comparison between a shear lag type model and an Eshelby type model in predicting the mechanical properties of a short fiber composite. *Scr. metall.* **21**, 349–354.

Taya, M. & Arsenault, R. J. 1989. *Metal Matrix Composites*. Pergamon Press, Oxford.

Tharp, T. M. 1983. Analogies between the high-temperature deformation of polyphase rocks and the mechanical behavior of porous powder metal. *Tectonophysics* **96**, T1–11.

Tullis, T. E., Horowitz, F. G. & Tullis, J. 1991. Flow laws of polyphase aggregates from end-member flow laws. *J. geophys. Res.* **96**, 8081–8096.

Twiss, R. J. 1977. Theory and applicability of a recrystallized grain size paleopiezometer. *Pure & Appl. Geophys.* **115**, 227–244.

Tyson, W. R. & Davies, G. J. 1965. A photoelastic study of the shear stresses associated with the transfer of stress during fiber reinforcement. *Br. J. appl. Phys.* **16**, 199–205.

Wu, Y. & Lavernia, E. J. 1992. Strengthening behavior of particulate reinforced MMCs. *Scr. metall. Mater.* **27**, 173–178.

Zhao, P. & Ji, S. 1992. Comment on "Strengthening Behavior of Particulate Reinforced MMCs" by Y. Wu and E. J. Lavernia, and "On the Strength of Discontinuous Silicon Carbide Reinforced Aluminum Composites" by V. C. Nardone and K. M. Prewo. *Scr. metall. Mater.* **27**, 1443.